Functional Nanostructures Hot Paper

International Edition: DOI: 10.1002/anie.201503017
German Edition: DOI: 10.1002/ange.201503017

A Universal Approach to Ultrasmall Magneto-Fluorescent Nanohybrids**

*Artur Feld, Jan-Philip Merkl, Hauke Kloust, Sandra Flessau, Christian Schmidtke, Christopher Wolter, Johannes Ostermann, Michael Kampferbeck, Robin Eggers, Alf Mews, Theo Schotten, and Horst Weller**

Abstract: *Seeded emulsion polymerization is a powerful universal method to produce ultrasmall multifunctional magnetic nanohybrids. In a two-step procedure, iron oxide nanocrystals were initially encapsulated in a polystyrene (PS) shell and subsequently used as beads for a controlled assembly of elongated quantum dots/quantum rods (QDQRs). The synthesis of a continuous PS shell allows the whole construct to be fixed and the composition of the nanohybrid to be tuned. The fluorescence of the QDQRs and magnetism of iron oxide were perfectly preserved, as confirmed by single-particle investigation, fluorescence decay measurements, and relaxometry. Biofunctionalization of the hybrids was straightforward, involving copolymerization of appropriate affinity ligands as shown by immunoblot analysis. Additionally, the universality of this method was shown by the embedment of a broad scale of NPs.*

Nanocrystals (NCs) are favorable materials for biomedical applications, which is mainly due to superparamagnetism, fluorescence, or plasmonic behavior.[1] This makes nanocrystals a platform for magnetic-resonance and fluorescence imaging as well as a scaffold for new therapeutic agents.[2] Usually three different types of nanocrystals are used that exhibit these properties: iron oxide,[3] semiconductors, and gold NCs.[4] CdSe/CdS/ZnS quantum dots (QDs) show high fluorescence quantum yields and photostability, which offers the opportunity to use them in various fluorescence imaging techniques.[5] Recently, elongated quantum dots in quantum rods (QDQRs) have gained more interest, because of their even higher fluorescence quantum yield, polarized emission, and enhanced multiphoton absorption.[6] A material combining magnetism, fluorescence, and/or plasmonic behavior is desirable because the bio-imaging techniques benefiting from these effects complement each other. Since no single material is known to have these combined properties, multifunctional composites were achieved by attaching different particles within one construct. Such constructs are often referred to be nanocomposites or nanohybrids.

Various approaches for dual, that is, magnetofluorescent imaging have been described. The nanocrystal hybrid can be formed by a direct clustering of the as-synthesized crystals,[7] by co-encapsulation of different types of nanocrystals, or conjugation of separate nanoconstructs.[8] In particular, the second approach holds high potential, because the nanocrystal properties can be optimized for the different imaging modalities independently. However, care has to be taken that no undesirable interactions within the nanohybrid abrogate these respective properties. For example, in a magnetofluorescent hybrid, the fluorescence of semiconductor nanocrystals can be quenched by iron oxide nanocrystals or iron ions released thereof and have therefore been rarely described.[9] Furthermore, hybrids may exceed inherent biological size limits by profuse clustering of the nanocrystals.[9b]

Recently, Bawendi and co-workers presented superstructures comprised of close-packed magnetic nanoparticle cores that were fully surrounded by a shell of fluorescent quantum dots. Each "supernanoparticle" consists of about 2000 nanocrystals with an overall diameter of about 100 nm.[10] These superstructures form very regular superlattice fringes, thus providing an inherently fixed monodisperse distribution. Although photoluminescence quantum yield (PLQY) was significantly reduced down to 12%, the sheer number of fluorescent CdSe/CdS quantum dots still allowed single particle tracking and suppressed blinking. However, the putative hepatobiliary accumulation of these particles and eventual release of high cadmium concentrations may pose toxicological risks to living structures.

Herein, we propose a novel two-step concept that is further developed from our recently reported seeded emulsion polymerization technique.[11] This technique already allowed us to co-encapsulate gold and iron oxide NCs without impairment of each other's physicochemical properties.

[*] A. Feld,[+] J.-P. Merkl,[+] Dr. H. Kloust, Dr. S. Flessau, Dr. C. Schmidtke, C. Wolter, Dr. J. Ostermann, M. Kampferbeck, R. Eggers, Prof. Dr. A. Mews, Prof. Dr. H. Weller
Institute of Physical Chemistry, University of Hamburg
Grindelallee 117, 20146 Hamburg (Germany)
E-mail: weller@chemie.uni-hamburg.de
Dr. J. Ostermann, Prof. Dr. A. Mews, Dr. T. Schotten, Prof. Dr. H. Weller
Center for Applied Nanotechnology
Grindelallee 117, 20146 Hamburg (Germany)
Prof. Dr. H. Weller
The Hamburg Center for Ultrafast Imaging, University of Hamburg
Luruper Chaussee 149, 22761 Hamburg (Germany)
[+] These authors contributed equally to this work.

[**] We thank Jenny Spöttel for supporting the preparative work. This work was supported by SFB 986M3 of the German Research Foundation (DFG), the Chemical Industry Fund, VCI: German Chemical Industry Association, and the German–American Fulbright Program.

Supporting information for this article (experimental section, design and characterization of the nanohybrids (TEM, DLS), TEM analysis of iron oxide/nickel platinum, iron oxide/iron oxide, iron oxide/gold hybrids, and quantification of the purification process; confocal fluorescence microscopy video of the magneto-fluorescent hybrids) is available on the WWW under http://dx.doi.org/10.1002/anie.201503017.

However, combining iron oxide and semiconductor NCs with the same procedure was less successful, leading to irreversible fluorescence quenching.[9b] In contrast, by the approach presented herein, the pristine fluorescent properties of the QDQRs are fully maintained. Moreover, the composition of the nanohybrid can be user-defined tuned from dyads to clusters containing 30–40 NPs with diameters ranging from 50 to 150 nm (DLS).

During step (I) towards the formation of these magneto-fluorescent hybrid structures, we encapsulated iron oxide nanocrystals in a polysorbate 80/polystyrene shell as reported before (Scheme 1 A→B).[11a] After purification, elongated

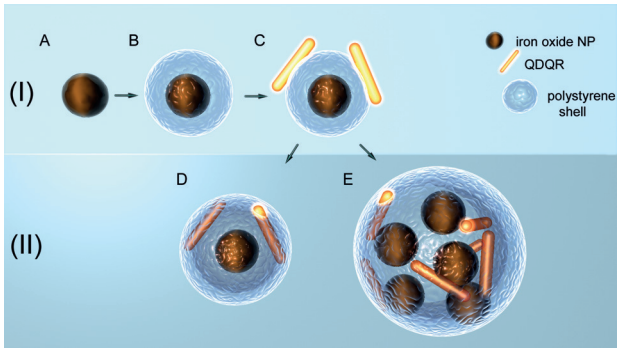

Scheme 1. The two-step hybrid formation. Step I: A) Iron oxide nanocrystals (native ligands not shown), B) iron oxide nanoparticles with the first polystyrene shell, C) nanohybrid after the deposition of QDQRs. Step II: D) nanohybrid after synthesizing a thin PS shell, E) nanohybrid after second emulsion polymerization, when dyads cluster owing to high styrene concentration.

QDQRs (CdSe/CdS) were deposited on the iron oxide-PS seeds by means of a controlled assembly. Although deposition of spherical NCs was considerably easier to achieve, we focused on the deposition of QDQRs owing to their advantages mentioned above. The assembly step (Scheme 1, B→C) determined the structure of the hybrids. The predominant formation of the dyads was controlled by injection speed, QDQR aspect ratio, QDQR/iron oxide NC ratio, as well as surface functionalization of the individual seed particles (see comprehensive discussion in the Supporting Information).

In brief, controlled deposition of QDQRs to the iron oxide beads was achieved by mixing a highly concentrated solution of the iron oxide–PS beads with QDQRs in THF, which was then rapidly injected into an aqueous solution of polysorbate 80. Owing to the increased polarity of the solution, the QDQR NCs attached to the polystyrene shell (B→C). Notably, QDQRs with aspect rations higher than 8 showed a propensity not to adhere to the PS shell, but arrange separately in a parallel fashion among themselves.

A consecutive emulsion polymerization was used to finally integrate this nanocomposite in a continuous PS shell optionally under functionalization with affinity ligands, for example, biotin (step II, C→D/E). This second step combines the established procedures[8] of co-encapsulation[11a] and conjugation[12] of different nanoparticles within one approach, which is very straightforward for the synthesis of an integrated, multifunctional nanohybrid with controlled surface properties. In step (II), low styrene and low NP concentrations yielded predominantly dyads (Figure 1a; DLS size 74 nm), whereas high styrene and NP concentrations led to multiply clustered hybrids (Figure 1b,c) with DLS size up to 150 nm. Remarkably, in most cases the ratio of QDQR/iron oxide was 1:1, suggesting that a primarily formed population of dyads assemble to higher clusters during the second polymerization step. For further investigations, samples consisting mainly of dyads were used.

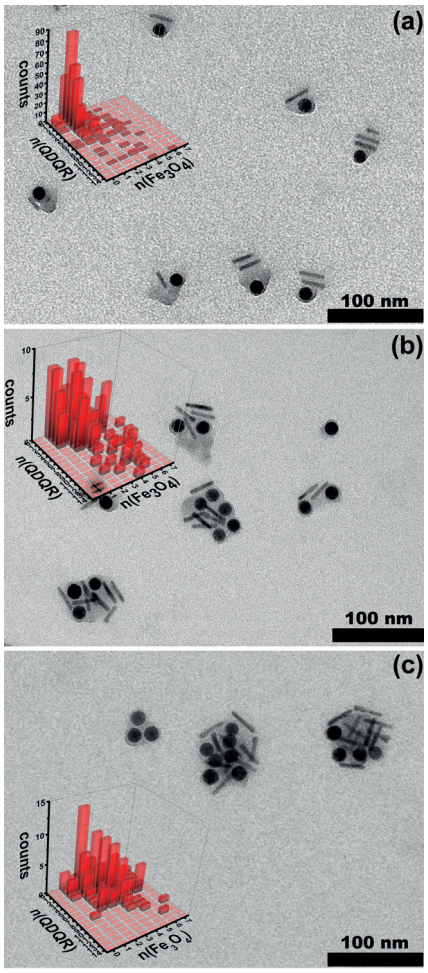

Figure 1. Representative TEM images of the different hybrids achieved using different amounts of monomer during the second emulsion polymerization. The inset shows a three-dimensional histogram of the number of QDQRs n(QDQR) and the number of iron oxide n(Fe_3O_4) within one hybrid. Amounts used of each monomer: a) 4 nmol, b) 8 nmol, c) 26 nmol.

Absorption and fluorescence properties of the hybrids are shown in Figure 2a and b. The absorption spectrum (black solid line) represents an exact superposition of the iron oxide (black dashed line) and of the QDQRs (red line) spectra, and the fluorescence spectrum is identical to the pure QDQRs. Owing to the strong light absorption of the iron oxide, standard measurements did not yield reliable values for the fluorescence quantum yield of the hybrids. However, considering the inner filter effect, the fluorescence intensities of the hybrids and the pure QDQRs were very similar.

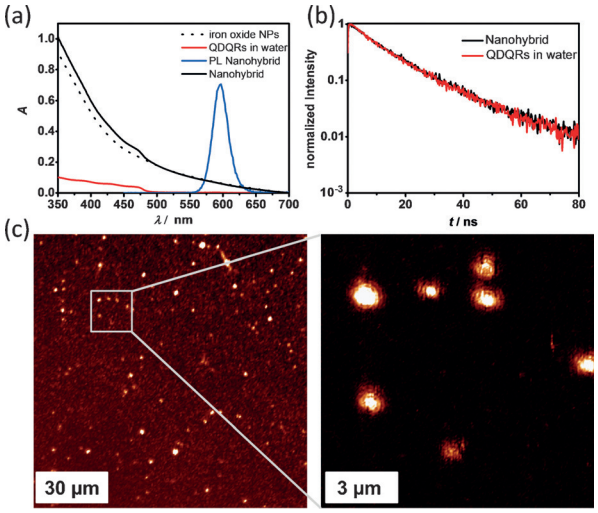

Figure 2. a) Absorption spectra of the hybrids (black solid line), absorption spectra of polystyrene encapsulated iron oxide nanocrystals (black dashed line), absorption spectra of QDQRs (red solid line), normalized emission spectra of the hybrids (blue solid line). b) Normalized fluorescence decay curves of the nanohybrids (black) and of the encapsulated QDQRs (red). c) Confocal fluorescence microscopy images of the individual hybrids.

Furthermore, we examined the fluorescence decay times of the QDQR–iron oxide hybrids in comparison to a pure QDQR sample. As can be clearly seen in Figure 2b, the fluorescence lifetime of the QDQRs (11 ns) does not change in the hybrids. We concluded that no interactions between the iron oxide NC and the QDQR exist, which would lead to dynamic quenching. An additional indication for the conservation of the fluorescence properties of the QDQRs within the hybrids was found in single-particle fluorescence investigations (Figure 2c).

The characterization of the fluorescence properties of the hybrids compared with those of the pure QDQRs by confocal techniques reflects biological conditions more accurately than cuvette measurements. In biological systems, samples are regularly highly diluted and have low section thicknesses, making light absorption by the iron oxide less disturbing.

We compared the average fluorescence intensities of the QDQR–iron oxide hybrid emission with those of a pure QDQR and found almost identical average values (10–15 particles counted; see the Supporting Information).

Remarkably, these dyad-hybrids exhibit fluorescence blinking, characteristic for single-particle fluorescence (video available in the Supporting Information). It should be noted that these features are indispensable for super resolution microscopy, such as STORM and related techniques.[13]

These results clearly indicate that the QDQRs in the hybrids were perfectly shielded against quenching agents and the average distance between QDQRs and iron oxide was large enough to suppress electron or energy transfer. The magnetic properties of the magnetofluorescent nanohybrids were measured by relaxometry at 1.41 T and 37 °C. With a r_2 relaxivity of 164 $mM^{-1}s^{-1}$, the hybrids exhibit typical values of T_2 or T_2* contrast agents for magnetic resonance imaging. Compared to solitarily encapsulated iron oxide nanocrystals by seeded emulsion polymerization, no significant changes in r_2 were observed. This clearly indicates that only one iron oxide nanocrystal per dyad was enclosed. In contrast, the T_2 relaxivity of the nanohybrid can be increased to 240 $mM^{-1}s^{-1}$ by synthesizing iron oxide/iron oxide core/satellite structures (see the Supporting Information). This increase may be explained by magnetic interactions leading to an enhancement of the saturation magnetization in the hybrids.[14]

As shown recently, seeded emulsion polymerization allows a concomitant co-polymerization of affinity molecules. Following this approach, biotin-PEO_{60}-*N*-(allyl 2-hydroxypropyl ether) was copolymerized during step (II).[15] In a dot-blot experiment, the biotinylated nanohybrids showed binding to NeutrAvidin, whereas the corresponding non-biotinylated probe showed none (see photograph in the Supporting Information).

To show the broad scope of this approach, we embedded spherical gold, nickel–platinum, iron oxide nanocrystals, and QDs (CdSe/CdS/ZnS) and synthesized a variety of multifunctional nanohybrids with biological relevance. The combination of iron oxide with nickel platinum nanocrystals may find applications in catalysis, where particles can be easily separated from the reaction mixture by simply applying a magnet.

In conclusion, consecutive seeded emulsion polymerization allows the preparation of advanced nanohybrids combining completely different properties without any interference of the uniform particles. Recently, we demonstrated that a PS shell is highly effective to prevent fluorescence quenching of singly encapsulated semiconductor NCs.[11b,16] Herein we expanded on these findings by embedding diverse nanocrystals into a continuous PS. The first PS shell efficiently insulates iron oxide NCs from QDQRs, thus suppressing effectively dynamic and static quenching. Furthermore, it also acts as an ion barrier, suppressing leaching of cadmium ions. The combined QDQRs/iron oxide magnetofluorescent nanohybrids fully preserved the fluorescence of the incorporated QDQRs. This method allows the synthesis of exceptional small nanohybrids with excellent properties, which is hardly achievable by other methods or one single material. Additionally, purification and bio-functionalization of the nanohybrids was very straightforward, as demonstrated by magnetic column purification and co-polymerization of a biotin monomer, respectively. These hybrids may spur major progress in targeted dual imaging applications.

Keywords: emulsion polymerization · magnetofluorescence · nanocomposites · nanohybrids · single-particle spectroscopy

How to cite: *Angew. Chem. Int. Ed.* **2015**, *54*, 12468–12471
Angew. Chem. **2015**, *127*, 12645–12648

[1] a) M. J. Sailor, J. H. Park, *Adv. Mater.* **2012**, *24*, 3779–3802; b) H. Goesmann, C. Feldmann, *Angew. Chem. Int. Ed.* **2010**, *49*, 1362–1395; *Angew. Chem.* **2010**, *122*, 1402–1437.
[2] Z. P. Qin, J. C. Bischof, *Chem. Soc. Rev.* **2012**, *41*, 1191–1217.
[3] a) N. Lee, T. Hyeon, *Chem. Soc. Rev.* **2012**, *41*, 2575–2589; b) D. Yoo, J.-H. Lee, T.-H. Shin, J. Cheon, *Acc. Chem. Res.* **2011**, *44*,

863 – 874; c) J. Gao, H. Gu, B. Xu, *Acc. Chem. Res.* **2009**, *42*, 1097 – 1107.

[4] a) R. A. Sperling, P. Rivera Gil, F. Zhang, M. Zanella, W. J. Parak, *Chem. Soc. Rev.* **2008**, *37*, 1896 – 1908; b) D. A. Giljohann, D. S. Seferos, W. L. Daniel, M. D. Massich, P. C. Patel, C. A. Mirkin, *Angew. Chem. Int. Ed.* **2010**, *49*, 3280 – 3294; *Angew. Chem.* **2010**, *122*, 3352 – 3366.

[5] a) T. Jamieson, R. Bakhshi, D. Petrova, R. Pocock, M. Imani, A. M. Seifalian, *Biomaterials* **2007**, *28*, 4717 – 4732; b) E. Pöselt, C. Schmidtke, S. Fischer, K. Peldschus, J. Salamon, H. Kloust, H. Tran, A. Pietsch, M. Heine, G. Adam, U. Schumacher, C. Wagener, S. Förster, H. Weller, *ACS Nano* **2012**, *6*, 3346 – 3355; c) G. Xu, K.-T. Yong, I. Roy, S. D. Mahajan, H. Ding, S. A. Schwartz, P. N. Prasad, *Bioconjugate Chem.* **2008**, *19*, 1179 – 1185; d) K.-T. Yong, I. Roy, H. E. Pudavar, E. J. Bergey, K. M. Tramposch, M. T. Swihart, P. N. Prasad, *Adv. Mater.* **2008**, *20*, 1412 – 1417.

[6] a) J. Dimitrijevic, L. Krapf, C. Wolter, C. Schmidtke, J. P. Merkl, T. Jochum, A. Kornowski, A. Schuth, A. Gebert, G. Huttmann, T. Vossmeyer, H. Weller, *Nanoscale* **2014**, *6*, 10413 – 10422; b) H. Htoon, J. A. Hollingworth, A. V. Malko, R. Dickerson, V. I. Klimov, *Appl. Phys. Lett.* **2003**, *82*, 4776 – 4778.

[7] a) S. T. Selvan, P. K. Patra, C. Y. Ang, J. Y. Ying, *Angew. Chem. Int. Ed.* **2007**, *46*, 2448 – 2452; *Angew. Chem.* **2007**, *119*, 2500 – 2504; b) N. s. Pazos-Pérez, Y. Gao, M. Hilgendorff, S. Irsen, J. Pérez-Juste, M. Spasova, M. Farle, L. M. Liz-Marzán, M. Giersig, *Chem. Mater.* **2007**, *19*, 4415 – 4422; c) N. Lee, H. R. Cho, M. H. Oh, S. H. Lee, K. Kim, B. H. Kim, K. Shin, T.-Y. Ahn, J. W. Choi, Y.-W. Kim, S. H. Choi, T. Hyeon, *J. Am. Chem. Soc.* **2012**, *134*, 10309 – 10312; d) L. Y. T. Chou, K. Zagorovsky, W. C. W. Chan, *Nat. Nanotechnol.* **2014**, *9*, 148 – 155.

[8] a) F. Erogbogbo, K. T. Yong, R. Hu, W. C. Law, H. Ding, C. W. Chang, P. N. Prasad, M. T. Swihart, *ACS Nano* **2010**, *4*, 5131 – 5138; b) N. Insin, J. B. Tracy, H. Lee, J. P. Zimmer, R. M. Westervelt, M. G. Bawendi, *ACS Nano* **2008**, *2*, 197 – 202; c) R. Kas, E. Sevinc, U. Topal, H. Y. Acar, *J. Phys. Chem. C* **2010**, *114*, 7758 – 7766; d) V. Roullier, F. Grasset, F. Boulmedais, F. Artzner, O. Cador, V. r. Marchi-Artzner, *Chem. Mater.* **2008**, *20*, 6657 – 6665; e) R. Di Corato, N. C. Bigall, A. Ragusa, D. Dorfs, A. Genovese, R. Marotta, L. Manna, T. Pellegrino, *ACS Nano* **2011**, *5*, 1109 – 1121; f) B.-S. Kim, T. A. Taton, *Langmuir* **2007**, *23*, 2198 – 2202; g) J.-H. Park, G. von Maltzahn, E. Ruoslahti, S. Bhatia, M. Sailor, *Angew. Chem. Int. Ed.* **2008**, *47*, 7284 – 7288; *Angew. Chem.* **2008**, *120*, 7394 – 7398.

[9] a) K. Boldt, S. Jander, K. Hoppe, H. Weller, *ACS Nano* **2011**, *5*, 8115 – 8123; b) N. C. Bigall, W. J. Parak, D. Dorfs, *Nano Today* **2012**, *7*, 282 – 296.

[10] O. Chen, L. Riedemann, F. Etoc, H. Herrmann, M. Coppey, M. Barch, C. T. Farrar, J. Zhao, O. T. Bruns, H. Wei, P. Guo, J. Cui, R. Jensen, Y. Chen, D. K. Harris, J. M. Cordero, Z. Wang, A. Jasanoff, D. Fukumura, R. Reimer, M. Dahan, R. K. Jain, M. G. Bawendi, *Nat. Commun.* **2014**, *5093*, 1 – 8.

[11] a) H. Kloust, E. Pöselt, S. Kappen, C. Schmidtke, A. Kornowski, W. Pauer, H.-U. Moritz, H. Weller, *Langmuir* **2012**, *28*, 7276 – 7281; b) H. Kloust, C. Schmidtke, J.-P. Merkl, A. Feld, T. Schotten, U. E. A. Fittschen, M. Gehring, J. Ostermann, E. Pöselt, H. Weller, *J. Phys. Chem. C* **2013**, *117*, 23244 – 23250.

[12] C. Schmidtke, H. Kloust, N. G. Bastús, J.-P. Merkl, H. Tran, S. Flessau, A. Feld, T. Schotten, H. Weller, *Nanoscale* **2013**, *5*, 11783 – 11794.

[13] T. Dertinger, R. Colyer, G. Iyer, S. Weiss, J. Enderlein, *Proc. Natl. Acad. Sci. USA* **2009**, *106*, 22287 – 22292.

[14] a) C. Schmidtke, R. Eggers, R. Zierold, A. Feld, H. Kloust, C. Wolter, J. Ostermann, J. P. Merkl, T. Schotten, K. Nielsch, H. Weller, *Langmuir* **2014**, *30*, 11190 – 11196; b) R. J. Hickey, A. S. Haynes, J. M. Kikkawa, S. J. Park, *J. Am. Chem. Soc.* **2011**, *133*, 1517 – 1525.

[15] H. Kloust, C. Schmidtke, A. Feld, T. Schotten, R. Eggers, U. E. A. Fittschen, F. Schulz, E. Pöselt, J. Ostermann, N. G. Bastús, H. Weller, *Langmuir* **2013**, *29*, 4915 – 4921.

[16] a) H. Kloust, C. Schmidtke, J. P. Merkl, A. Feld, T. Schotten, U. E. A. Fittschen, M. Gehring, J. Ostermann, E. Poselt, H. Weller, *J. Phys. Chem. C* **2013**, *117*, 23244 – 23250; b) J. Ostermann, C. Schmidtke, C. Wolter, J. P. Merkl, H. Kloust, H. Weller, *Beilstein J. Nanotechnol.* **2015**, *6*, 232 – 242; c) J. Ostermann, J. P. Merkl, S. Flessau, C. Wolter, A. Kornowksi, C. Schmidtke, A. Pietsch, H. Kloust, A. Feld, H. Weller, *ACS Nano* **2013**, *7*, 9156 – 9167.

Received: April 1, 2015
Revised: April 30, 2015
Published online: July 2, 2015

